JOURNAL OF MATERIALS SCIENCE 33 (1998) 5795–5801

Preparation and mechanical properties of Al_2O_3 reinforced by submicrometer Co particles

W. P. TAI, T. WATANABE
Department of Inorganic Composite Materials, Kyushu National Industrial Research Institute, Tosu, Saga 841-0052, Japan
E-mail: tai@kniri.go.jp

Al_2O_3/Co composites were fabricated by vacuum hot-pressing a mixture of α-Al_2O_3 powder and a fine cobalt powder. Submicron-sized cobalt particles were uniformly dispersed into the Al_2O_3 matrix, and the dispersed type was a more inter-/intragranular one with increases of cobalt content up to 40 wt % Co addition. The growth of cobalt particles occurred with increasing cobalt content. At 50 wt % Co addition, however, the growth as well as coalescence of cobalt particles occurred. The phases formed in the Al_2O_3/Co composites were f-Co(fcc), h-Co(hcp), α-Al_2O_3, and a small amount of graphite. Significant improvements in bending strength (from 341 to 771 MPa) and fracture toughness (from 3.7 to 6.7 MPa $\cdot$ $m^{1/2}$) of the Al_2O_3/40 wt % Co(23 vol % Co) composite compared to monolithic Al_2O_3 were achieved by dispersing submicron-sized Co particles into the Al_2O_3 matrix. The improvement in bending strength was attributed to the compressive thermal residual stress in the matrix Al_2O_3 induced by the mismatch of the coefficients of thermal expansion (CTE) between the matrix Al_2O_3 grains and cobalt particles during cooling from hot-pressing temperature. The fracture toughness of the composite was enhanced by crack bridging, crack deflection, and compressive thermal residual stress.

1. Introduction

Alumina ceramic possesses high refractory capabilities, good wear resistance, and chemical stability. Its application as a structural material, however, is limited by its low fracture toughness which can hardly alleviate stress concentration by applied stress resulting from a surface flaw or internal flaw. Many attempts have been made to create ceramic matrix composites by dispersing metal [1, 2] and ceramic second particles [3, 4] into the Al_2O_3 matrix for improved mechanical properties. Recently, nanocomposites [5–7] have been developed to improve the mechanical properties, providing increase of strength with slight improvement of fracture toughness. The dispersions of nano-sized ceramic particles into the ceramic matrix are more widely studied than those of metal particles. It is shown that the dispersions of ceramic particles into the ceramic matrix are more notably enhanced in strength with slight improvement in fracture toughness than those of metal particles, and the coefficient of thermal expansion (CTE) of the dispersed particle (α_d) then is smaller than that of the matrix grain (α_m). Pezzotti *et al.* [8], however, argued that the inherent increase of toughness in the nanocomposite was physically limited. On the other hand, when the CTE of the reinforced particle exceeds that of the matrix, the compressive thermal residual stress in the bulk of the matrix is generated, and the resultant toughening of the composite is caused by compressive thermal residual stress [9]. Virkar and Johnson [10] also showed that thermal residual stress can enhance the fracture toughness of ceramic/metal composites. Faber and Evans [11, 12] accounted for toughening due to crack deflection through theory and experiment. Wei and Becher [13] also considered thermal residual stress as a major cause for the crack deflection. Budiansky *et al.* [14] reported the toughening of particulate-reinforced ceramics by the bridging of ductile metal particulates. In the system Al_2O_3/Co, the CTE of cobalt is larger than that of Al_2O_3. Furthermore, the cobalt metal occur a martensitic transformation of f-Co(fcc, high-temperature phase) phase to h-Co(hcp, low-temperature phase) at 417 °C during cooling [15].

In the present study, Al_2O_3/Co composites were fabricated by dispersing submicron-sized cobalt particles into the Al_2O_3 matrix, and the mechanical properties of those resultant composites were investigated. The effects of a compressive thermal residual stress and the phase transformation of dispersed cobalt particles into the Al_2O_3 matrix for the mechanical properties also were investigated.

2. Experimental procedure

2.1. Sample preparation

The starting materials for the present investigation were α-Al_2O_3 powder (AKP-53, Sumitomo Chemical Co., Japan) of 0.2 μm and cobalt powder (Nilaco Co., Japan) of 0.03 μm in an average particle size. Al_2O_3/Co

powder mixtures containing 5 to 50 wt % Co were mixed with methanol and ethylene glycol (1 : 1 volume fraction) in an agate mill for 20 min. The mixed powders were immediately packed into graphite dies with an inside diameter of 12 mm. Specimens were hot-pressed in vacuum under a pressure of 20 MPa for 1 h at 1200 °C to 1360 °C. For comparison, a monolithic Al_2O_3 specimen was fabricated using the same method and the same sized powders. Al_2O_3/10 wt % Co composite also was fabricated using 2-μm α-Al_2O_3 powder and 2-μm cobalt powder.

2.2. Measurements and analyses

For microstructural observation, the specimens were cut and ground using a diamond wheel and then ground with SiC abrasive paper, followed by polishing with diamond paste (1, 3 μm) and lapping oil. The microstructures of the resulting composites and crack paths produced by a Vickers indenter were observed by scanning electron microscopy (SEM, JEOL JSM-6400K). Additionally, microstructural characteristics were examined by transmission electron microscopy (TEM, JEOL JEM-200CX). X-ray diffraction (XRD, RIGAKU RAD-2) analyses were conducted using Cu Kα radiation to determine the phases in the composites, and the surfaces of the composites also were X-rayed in the as-sintered, as-ground, and annealed conditions. Here, the as-sintered and annealed surfaces were ground using SiC abrasive paper (#100) to evaluate stress (strain)-induced transformation of Co phase [15] by the same method as ZrO_2 [16]. The f-Co and h-Co fraction in the composites were calculated using the f-Co and h-Co peak intensities. The porosity of the composites was measured by stereological point analysis from photographs taken at three areas of cross section using SEM. The grain size was estimated by the line intercept method after a thermal etching and in particular, the size of cobalt particle was measured on cobalt particles located at the Al_2O_3 matrix grain boundary. The bending strength was measured through a three-point bending test. The strength after annealing treatment also was measured to evaluate the relaxation of thermal residual stress [17] from the difference of the as-sintered (as-hot-pressed) and annealed composites. Annealing treatment was conducted in Ar atmosphere for 1 h at 1000 °C. The sample number used in each strength test was more than six. The fracture toughness (K_{IC}) and Vickers hardness (H_V) were evaluated by measuring the lengths of the cracks and impression diagonals generated by a Vickers indenter at a load of 196 N and a loading duration of 30 s [18]. K_{IC} and H_V tests were repeated at least 6 times. The error bars of each of the mechanical properties were exhibited minimum and maximum values.

3. Results and discussion

3.1. Formation of Al_2O_3/Co composites

Fig. 1 shows microstructures of Al_2O_3/Co composites hot-pressed at a temperature of 1270 °C for 1 h in vacuum. The cobalt particles were uniformly dispersed into the Al_2O_3 matrix. In addition, TEM images of

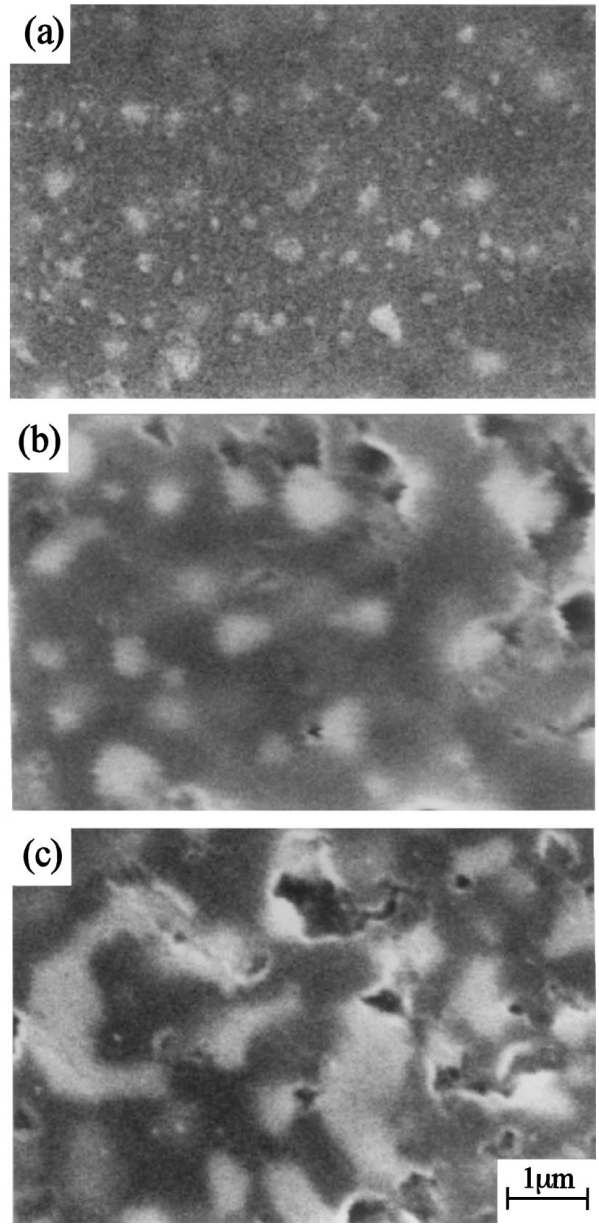

Figure 1 Scanning electron micrographs of the composites: (a) Al_2O_3/10 wt % Co, (b) Al_2O_3/40 wt % Co and (c) Al_2O_3/50 wt % Co.

Al_2O_3/10 wt % Co and Al_2O_3/40 wt % Co composites are shown in Fig. 2 and then the arrows indicate Co phases. In the Al_2O_3/10 wt % Co composite, the cobalt particles were dispersed particularly at the matrix grain boundary, intergranular type. In the Al_2O_3/40 wt % Co composite, however, the cobalt particles were more dispersed both at the matrix grain boundary and within the Al_2O_3 grains, intergranular/intragranular type. The dispersed cobalt particles then exhibited submicrometer order. Fig. 3 shows the average sizes of cobalt particles located at the matrix grain boundary and the grain sizes of Al_2O_3. The growth of cobalt particles occurred with increasing cobalt content up to 40 wt % Co addition. In the case of Al_2O_3/50 wt % Co composite with much more Co amount, however, growth as well as coalescence of cobalt particles occurred. The coalescence of Co particles in the Al_2O_3/50 wt % Co composite may have resulted from agglomeration of Co particles due to the addition of much more Co during mixing in an agate mill. In the Al_2O_3 grain size, on the other hand,

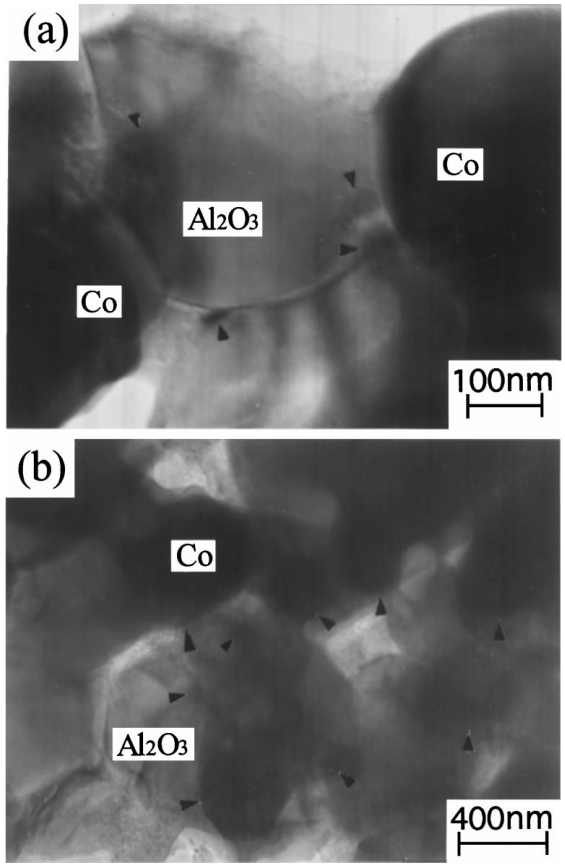

Figure 2 TEM micrographs showing the microstructure of the Al_2O_3/10 wt % Co composite(a) and of the Al_2O_3/40 wt % Co composite(b). The dispersed Co particles are indicated by arrows.

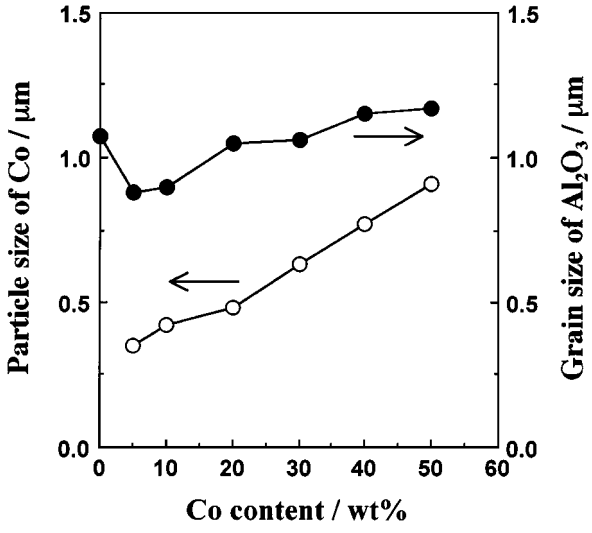

Figure 3 Sizes of Al_2O_3 grains and of Co particles as function of Co content in Al_2O_3/Co composites.

the addition of cobalt particles resulted in the inhibition of grain growth of Al_2O_3 in the matrix, which exhibited smaller grain size than monolithic Al_2O_3 up to 30 wt % Co addition. Fig. 4 shows the porosity of the Al_2O_3/Co composites along with the Co content. The average porosity obtained from three areas of cross section then was 1.62 to 2.87 vol %.

The phases formed in the Al_2O_3/Co composites were f-Co, h-Co, α-Al_2O_3, and a small amount of C(graphite), as shown in Fig. 5. In order to find the

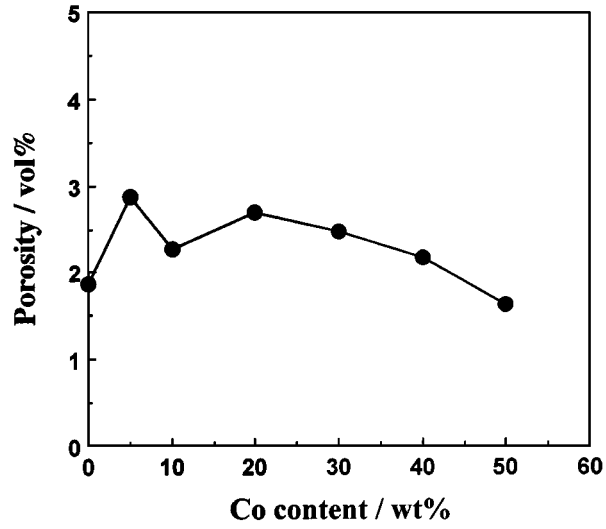

Figure 4 Porosity of Al_2O_3/Co composites.

cause of graphite formation, both Al_2O_3 powder alone and the Al_2O_3 powder containing methanol and ethylene glycol (1 : 1 volume fraction) were hot-pressed in graphite dies. As a result, a small amount of graphite formed in both. The formation of the small amount of graphite was attributed to diffusion of carbon from the graphite die during hot-pressing.

3.2. Mechanical properties of Al_2O_3/Co composites

First, to determine the optimum hot-pressing temperature, changes in the mechanical properties of Al_2O_3/Co composites containing 10 wt % Co were investigated with hot-pressing temperature for 1 h in vacuum, and the results shown in Fig. 6. The bending strength showed a maximum value at the hot-pressing temperature of 1270 °C. Fracture toughness decreased with increasing hot-pressing temperature. The Vickers hardnesses of the hot-pressed composites were 20.26 GPa at 1200 °C, 20.34 GPa at 1270 °C, and 18.56 GPa at 1360 °C. Because those values indicated that the bending strength, fracture toughness and Vickers hardness of composites fabricated at 1270 °C were superior to those of composites fabricated at the other temperatures, all hot-pressing thereafter was performed at 1270 °C. On the other hand, hot-pressing using 2-μm α-Al_2O_3 powder and 2-μm cobalt powder (10 wt % Co) was not easily sintered even at the hot-pressing temperature of 1360 °C. The mechanical properties of hot-pressed samples at 1450 °C for 1 h were 318 MPa in bending strength, 4 MPa $\cdot$ $m^{1/2}$ in fracture toughness and 16.33 GPa in Vickers hardness.

Fig. 7 shows the bending strength of Al_2O_3/Co composites hot-pressed at 1270 °C as a function of cobalt content. The bending strength increased notably as the content of cobalt is increased, reaching a peak value at the addition of 40 wt % Co, from 341 MPa of monolithic Al_2O_3 to 771 MPa. However, it decreased to 564 MPa upon the addition of 50 wt % Co. In the present system Al_2O_3/Co composites, the thermal residual stress induced by the CTE mismatch between the matrix Al_2O_3 grains (8.4×10^{-6} °C^{-1}) and the dispersed cobalt

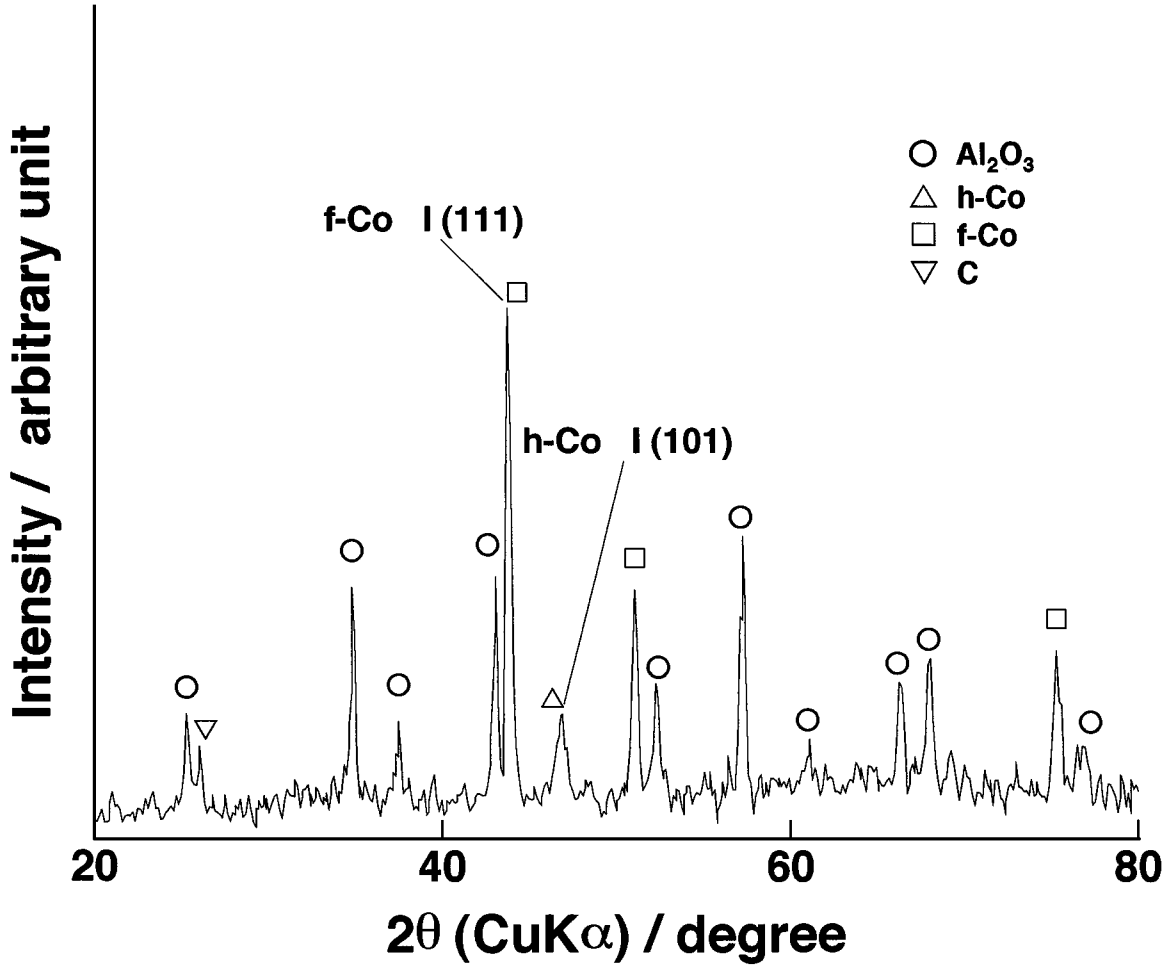

Figure 5 XRD pattern of Al_2O_3/40 wt % Co composite.

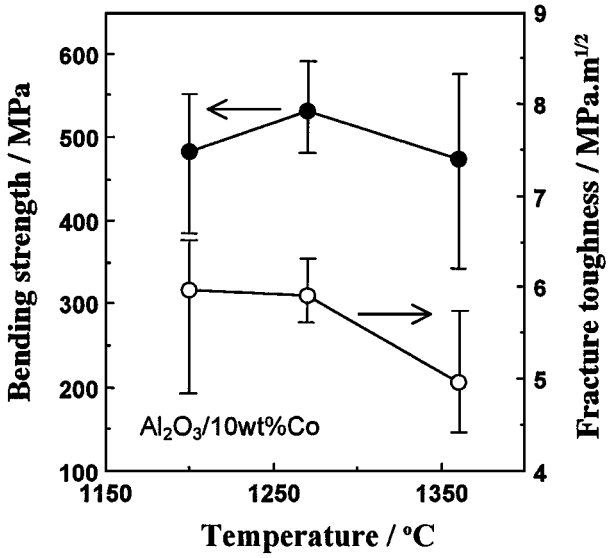

Figure 6 Mechanical properties with temperature for hot-pressed Al_2O_3/Co composites.

particles (13.36×10^{-6} °C^{-1}) during cooling down from the hot-pressing temperature can be envisaged in the viewpoint of intragranular and intergranular type. In the case of the dispersion of submicron-sized cobalt particles within the Al_2O_3 grains (intragranular type), hydrostatic tensile stress is produced in the cobalt particle because of the larger CTE of the dispersed particle than that of the matrix grain. The result is compressive stress in the Al_2O_3 matrix. In the case of the dispersion of cobalt particles at the Al_2O_3 matrix grain boundary (intergranular type), on the other hand, a high compressive residual stress in the bulk of the matrix Al_2O_3 and a low tensile stress at the dispersed cobalt particles are induced by the higher CTE of cobalt than that of Al_2O_3 during cooling down from the hot-pressing temperature [9]. In the hot-pressed Al_2O_3/Co composite that Co particles disperse within Al_2O_3 grains and at the Al_2O_3 matrix grain boundary, compressive thermal residual stress occurs in the bulk of Al_2O_3 matrix. The decrease (relaxation) of the residual stress then corresponds to the difference of as-sintered (as-hot-pressed) bending strength and annealed bending strength, as shown in Table I. Al_2O_3/40 wt % Co composite which dispersed into much more inter/intragranular type without the coalescence of cobalt particles occurred the higher compressive thermal residual stress, as explained.

Furthermore, the compressive residual stress in the Al_2O_3 can be produced by a phase transformation of high-temperature metastable fcc to low-temperature stable hcp of cobalt metal during cooling, although the mixtures of fcc and hcp normally coexist even at room temperature. Table I shows the h-Co fraction of the as-sintered, annealed and ground conditions in the composites using the peak intensities of f-Co and h-Co phases in Fig. 5. In the case of Al_2O_3/40 wt % Co compared to Al_2O_3/10 wt % Co composite, the h-Co

TABLE I Phase variations and mechanical properties for different conditions

Specimens	Conditions	h-Co fraction (%)	Bending strength (MPa)	Fracture toughness ($MPa \cdot m^{1/2}$)	Hardness (GPa)
Al_2O_3/10Co	as-sintered	10.2	531	5.89	20.34
Al_2O_3/10Co	ground^{+}	12.2	—	—	—
Al_2O_3/10Co	annealed^{++}	5.3	495	3.88	19.67
Al_2O_3/10Co	ground^{+++}	15.8	—	—	—
Al_2O_3/40Co	as-sintered	25.7	771	6.69	15.04
Al_2O_3/40Co	ground^{+}	43.5	—	—	—
Al_2O_3/40Co	annealed^{++}	16.7	544	3.9	13.36
Al_2O_3/40Co	ground^{+++}	41.9	—	—	—

$^{+}$Samples were ground using SiC abrasive paper (#100) after sintering. $^{++}$Samples were annealed in Ar for 1 h at 1000 °C after sintering. $^{+++}$Samples were ground after annealing.

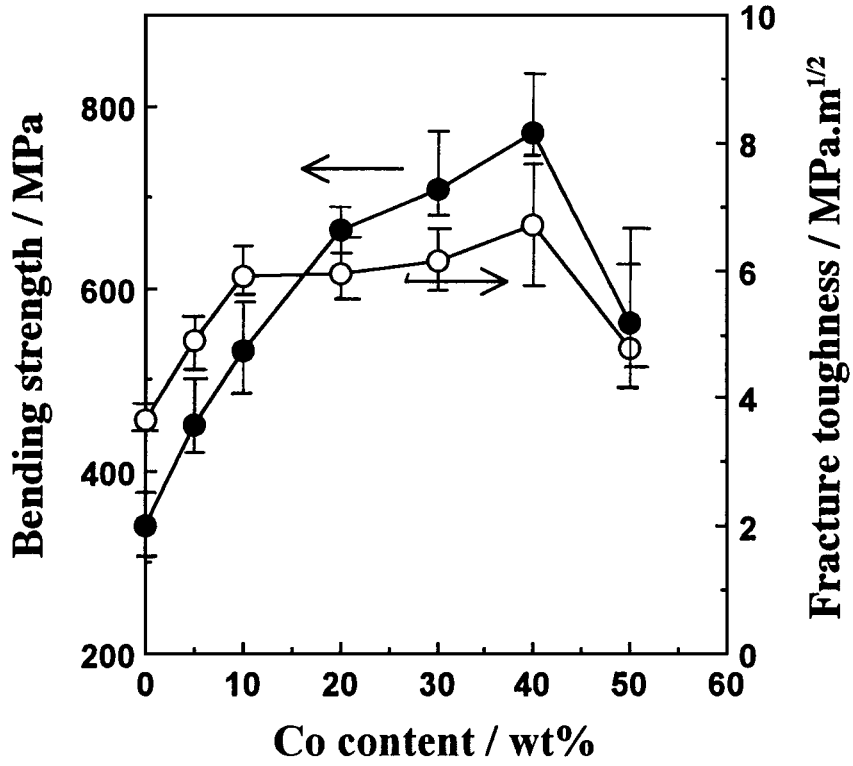

Figure 7 Mechanical properties with Co content for Al_2O_3/Co composites.

fraction of the as-sintered condition is larger. On the other hand, the h-Co fraction in the annealed condition compared to the as-sintered one decreased, which is related to the reverse phase transformation, and both composites then decreased in bending strength. The phase transformation of f-Co to h-Co, however, was occurred by grinding as-sintered and annealed surfaces in both composites, that is, stress (or strain)-induced transformation at the instant of fracture [15, 16], and the amount of phase transformation in the annealed conditions then was larger than that in the as-sintered ones, despite decreases of bending strength in annealed conditions. This implies that the phase transformation does not play a major role in the improvement of bending strength. The thermal residual stress thus was relieved during cooling slowly from and keeping at the annealing temperature, and the relaxation values of compressive thermal residual stresses (-36 MPa for Al_2O_3/10 wt % Co and -227 MPa for Al_2O_3/40 wt % Co composite) then are the difference of the as-sintered bending strength and annealed bending strength [17] as shown in Table I. Here, the cooling under hot-pressing was done quite rapidly from the hot-pressing temperature; the cooling under annealing was done slowly from the annealing temperature.

Pohanka *et al.* [19] introduced a term of internal stress in fracture mechanics, which added internal stress to applied stress, as follows:

$$\sigma = \sigma_{\text{applied}} + \sigma_{\text{internal}} = \text{Y}(\text{E}\gamma/\text{a})^{1/2} \qquad (1)$$

where σ is fracture stress, E is Young's modulus, γ is fracture energy, a is flaw size, and Y is geometrical constant (1.12 for semicircular flaws). Equation (1) can be derived as follows:

$$\sigma_{\text{applied}} = 0.8\text{K}_{\text{IC}}/\text{a}^{1/2} - \sigma_{\text{internal}} \qquad (2)$$

where $\text{K}_{\text{IC}} = (2\text{E}\gamma)^{1/2}$. In the case of acting compressive residual stress in the Al_2O_3, the applied stress could be added as much as compressive thermal residual stress, as shown in equation (2). From the viewpoint

of the inherent physical flaw sizes (10 to 50 μm) [20] rather than the critical flaw sizes (1 to 10 μm) in the present system, the term ($0.8\ K_{IC}/a^{1/2}$) in annealed samples was calculated by supposing the inherent flaw size of 30 μm. The values then were 564 MPa and 567 MPa in the Al_2O_3/10 wt % Co and Al_2O_3/40 wt % Co composite, respectively. The $\sigma_{applied}$ (i.e., as-sintered bending strength) in the Al_2O_3/10 wt % Co and Al_2O_3/40 wt % Co composites was obtained as 600 MPa and 794 MPa, respectively, by adding compressive thermal residual stress. The theoretical strength predicted from the relaxation value of residual stress was very close to the measured bending strength. The increase of bending strength with increasing cobalt content up to 40 wt % Co addition, i.e., more than two times higher than that of monolithic Al_2O_3, thus was attributed to the increase of compressive thermal residual stress induced by the mismatch in CTE of the matrix Al_2O_3 grains and submicron-sized Co particles.

The fracture toughness of Al_2O_3/Co composites with cobalt content is shown in Fig. 7. The fracture toughness increased continuously with increase of cobalt content, reaching a peak value at 40 wt % Co addition, and upon further increases the fracture toughness was decreased. XRD analyses were carried out to investigate the effect of the phase transformation in the as-sintered, annealed, and their respective ground conditions on the fracture toughness of the Al_2O_3/10 wt % Co and Al_2O_3/40 wt % Co composites, as shown in Table I. In both composites, the small amount of phase transformation of f-Co phase to h-Co occurred by grinding as-sintered specimen, and the h-Co fraction in Al_2O_3/40 wt % Co composite then was larger. This implies that the f-Co phase transforms into h-Co phase at the instant of fracture, i.e., stress (strain)-induced transformation [15, 16], even though the phase transformation by their incorporation occurred to some of degree because the submicron-sized cobalt particles were almost disconnectly dispersed into the Al_2O_3 matrix. The fracture toughness in the Al_2O_3/10 wt % Co and Al_2O_3/40 wt % Co composites of as-sintered conditions, however, was notably decreased by annealing treatment as shown in Table I, even though the fractions of phase transformation in the annealed conditions were larger than those in as-sintered conditions by grinding. The decrease of fracture toughness in the annealed condition thus seemed attributable to the relaxation of residual stress during cooling slowly from and keeping at annealing temperature. Taya *et al.* [9] confirmed that the compressive thermal residual stress in the bulk of the matrix was generated when the CTE of the particulate exceeded that of the matrix. In the system Al_2O_3/Co composites, the toughening of the composites was caused by compressive thermal residual stress [10].

The crack paths introduced by a Vickers indenter onto the polished surfaces of the Al_2O_3/5 wt % Co and Al_2O_3/40 wt % Co composites are shown in Fig. 8. In the Al_2O_3/5 wt % Co composite, a plane of crack propagation was almost straight. In the Al_2O_3/40 wt % Co composite with much more cobalt content, however, the crack propagated nonlinearly by crack deflection [12], and crack bridging also occurred [14]. According to

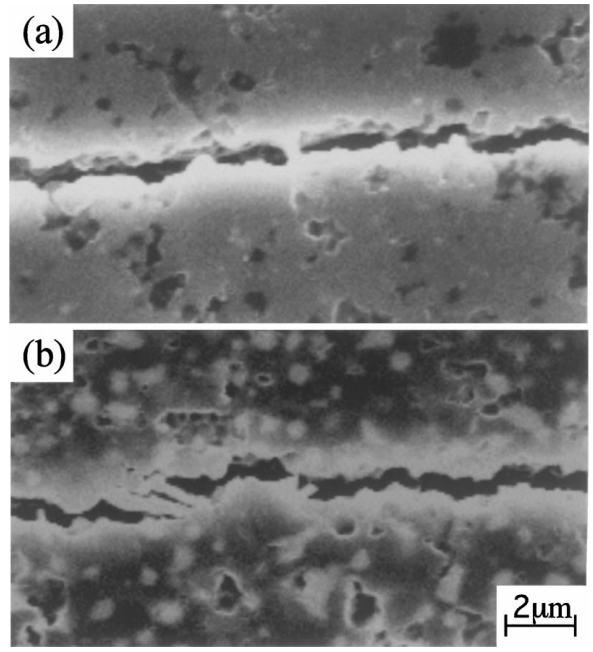

Figure 8 Crack profiles introduced by indentation: (a) Al_2O_3/5 wt % Co and (b) Al_2O_3/40 wt % Co composites.

Faber and Evans [12], crack deflection is commonly observed in brittle materials associated either with crack attraction or repulsion by second phase particles due to residual strains or with the presence of low bonding interface. Becher [21] reported that when the CTE of the reinforcement was larger than the CTE of the matrix, the tensile radial stresses acting on the interface of the matrix and reinforcement promoted debonding, and the interfacial debonding was necessary to achieve crack bridging. The submicron-sized cobalt particles in the Al_2O_3/40 wt % Co composite was crack bridged by the plastic deformation of the ductile particles, and the particle size then was larger than that in Al_2O_3/5 wt % Co composite, even though crack opening length at the region behind a crack tip in Al_2O_3/40 wt % Co composite was as large as the particle size of cobalt. The increased fracture toughness of the Al_2O_3/40 wt % Co composites thus was caused by crack bridging, crack deflection, and compressive thermal residual stress. In the Al_2O_3/50 wt % Co composite, on the other hand, growth as well as coalescence of cobalt particles occurred, as shown in Fig. 1(c). The decreased fracture toughness of the Al_2O_3/50 wt % Co composite may have resulted from the decrease of compressive thermal residual stress in the bulk of Al_2O_3 matrix due to the coalescent cobalt particles.

Fig. 9 shows the Vickers hardness values of Al_2O_3/Co composites with the addition of cobalt. The hardness attained a maximum of 20.97 GPa with the dispersion of 5 wt % Co, and its value decreased with increasing cobalt content, which approximately obeyed the rule of mixtures [7]. The hardening in the Al_2O_3/5 wt % Co composite resulted from the dispersion of lower cobalt content and smaller grain size [15]. The decrease in hardening with much larger amounts of cobalt could be attributed to the growth and coalescence of cobalt particles, and the decrease of Al_2O_3 content.

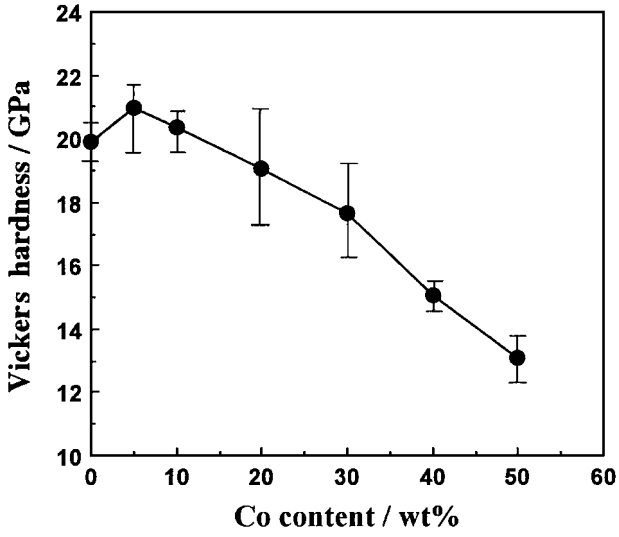

Figure 9 Vickers hardness with Co content for Al_2O_3/Co composites.

4. Conclusions

Al_2O_3/Co composites were fabricated by vacuum hot-pressing a mixture of α-Al_2O_3 powder and a fine cobalt powder. In the system Al_2O_3/Co, the submicron-sized cobalt particles were uniformly dispersed into the Al_2O_3 matrix, and were more dispersed into inter-/intragranular type with increases of cobalt content up to 40 wt % Co addition. The growth of cobalt particles took place with increasing cobalt content, particularly the coalescence of cobalt particles at 50 wt % Co addition. The phases of composites consisted of f-Co, h-Co, α-Al_2O_3, and a small amount of C. Bending strength and fracture toughness requirements can be satisfied simultaneously by dispersing submicron-sized cobalt particles into the Al_2O_3 matrix for an Al_2O_3/40 wt % Co composite. On the contrary, the Vickers hardness of composites except Al_2O_3/5 wt % Co composite decreased with increasing cobalt metal content.

Acknowledgement

This work was supported by the Research Development Corporation of Japan (JRDC) with a subsidy of Science and Technology Agency (STA) fellowship. One of the authors (Weon-Pil Tai) would also like to thank JRDC for its financial support. The authors also wish to acknowledge Dr. K. Shobu, Dr. H. Tateyama, and Mrs. K. Nishikubo at KNIRI for SEM and TEM observation, and Prof. T. Watari at Saga University for beneficial discussion.

References

1. C. O. MCHUGH, T. J. WHALEN and M. HUMENIK, JR. *J. Am. Ceram. Soc.* **49** (1996) 486.
2. W. H. TUAN and R. J. BROOK, *J. Eur. Ceram. Soc.* **6** (1990) 31.
3. N. CLAUSSEN, J. STEEB and R. F. PABST, *Am. Ceram. Soc. Bull.* **56** (1977) 559.
4. C. S. HWANG, Y. J. CHANG and S. W. CHEN, *J. Ceram. Soc. Jpn.* **104** (1996) 1.
5. K. NIIHARA, *J. Ceram. Soc. Jpn.* **99** (1991) 974.
6. L. C. STEARNS, J. ZHAO and M. P. HARMER, *J. Eur. Ceram. Soc.* **10** (1992) 473.
7. M. NAWA, T. SEKINO and K. NIIHARA, *J. Mater. Sci.* **29** (1994) 3185.
8. G. PEZZOTTI, T. NISHIDA and M. SAKAI, *J. Ceram. Soc. Jpn.* **103** (1995) 901.
9. M. TAYA, S. HAYASHI, A. S. KOBAYASHI and H. S. YOON, *J. Am. Ceram. Soc.* **73** (1990) 1382.
10. A.V. VIRKAR and D.L. JOHNSON, *J. Am. Ceram. Soc.* **60** (1977) 514.
11. K. T. FABER and A. G. EVANS, *Acta Metall.* **31** (1983) 565.
12. K. T. FABER and A. G. EVANS, *Acta Metall.* **31** (1983) 577.
13. G. C. WEI and P. F. BECHER, *J. Am. Ceram. Soc.* **67** (1984) 571.
14. B. BUDIANSKY, J. C. AMAZIGO and A.G. EVANS, *J. Mech. Phys. Solids* **36** (1988) 167.
15. H. SUZUKI, "Refractory Hard Metal and Sintered Hard Materials: Basics and Application" (Maruzen, Tokyo, 1986).
16. N. CLAUSSEN, *J. Am. Ceram. Soc.* **61** (1978) 85.
17. J. M. POTTER and R. A. MILLARD, in "Advances in X-Ray Analysis," Vol. 20, 1977, edited by H. F. Mcmurdie, C. S. Barrett, J. B. Newkirk and C. O. Ruud (Plenum Press, 1977) p. 309.
18. K. NIIHARA, *Bull. Ceram. Soc. Jpn.* **20** (1985) 12.
19. R. C. POHANKA, R. W. RICE and B. E. WALKER, JR., *J. Am. Ceram. Soc.* **59** (1976) 71.
20. G. PEZZOTTI, V. SERGO, K. OTA, O. SBAIZERO, N. MURAKI, T. NISHIDA and M. SAKAI, *J. Ceram. Soc. Jpn.* **104** (1996) 497.
21. P. F. BECHER, *J. Ceram. Soc. Jpn.* **99** (1991) 993.

Received 1 December 1997
and accepted 15 July 1998